remote sensing

MDPI

Article

Texture Features Derived from Sentinel-2 Vegetation Indices for Estimating and Mapping Forest Growing Stock Volume

Gengsheng Fang [1,2], Xiaobing He [3], Yuhui Weng [4] and Luming Fang [1,2,*]

[1] College of Mathematics and Computer Science, Zhejiang A & F University, Hangzhou 311300, China
[2] Key Laboratory of Forestry Intelligent Monitoring and Information Technology Research of Zhejiang Province, Zhejiang A & F University, Hangzhou 311300, China
[3] Baishanzu Scientific Research Monitoring Center, Qianjiangyuan-Baishanzu National Park, Lishui 323000, China
[4] College of Forestry and Agriculture, Stephen F. Austin State University, Nacogdoches, TX 75962, USA
* Correspondence: flming@zafu.edu.cn

Abstract: Forest growing stock volume (GSV, m^3/ha) is an indispensable variable for forest resources supervision. Precise measurement of GSV is conducive to monitoring forest dynamics. Nevertheless, little research has explored the pattern pixel values and the function of texture features derived from a vegetation index (VI) for GSV prediction. In this study, we investigated combining linear regression or Random Forest with Sentinel-2 spectral predictors and image textures derived from spectral bands and vegetation indices, which were based on standard deviation values or mean values at the plot level, for predicting GSV of Masson pine, theropencedrymion and all the survey plots in Anji County, China. Specifically, ten groups of experiments encompassing combinations of spectral parameters and texture measures were established for detecting the potential of image textures based on two different image pixel statistics. The results showed that texture measures derived from VI were superior to spectral parameters or texture measures derived from spectral bands for estimating the GSV of single tree species. Moreover, texture features based on shortwave infrared bands or their related VI and the standard deviation at pixel level for spectral bands/indices were emphasized. Finally, the mean value at the plot level exhibited slightly stronger potential than the standard deviation in general.

Keywords: GSV; texture measures; vegetation index; mean statistics; standard deviation

check for updates

Citation: Fang, G.; He, X.; Weng, Y.; Fang, L. Texture Features Derived from Sentinel-2 Vegetation Indices for Estimating and Mapping Forest Growing Stock Volume. *Remote Sens.* **2023**, *15*, 2821. https://doi.org/10.3390/rs15112821

Academic Editor: Dino Ienco

Received: 22 March 2023
Revised: 21 May 2023
Accepted: 26 May 2023
Published: 29 May 2023

Copyright: © 2023 by the authors. Licensee MDPI, Basel, Switzerland. This article is an open access article distributed under the terms and conditions of the Creative Commons Attribution (CC BY) license (https://creativecommons.org/licenses/by/4.0/).

1. Introduction

Forest growing stock volume (GSV, m^3/ha), which represents the volume of the total tree stems for all living species per unit [1], is a crucial element in the context of potent forest resource management. GSV is also closely connected with the estimation of aboveground biomass (AGB) and forest carbon storage [2]. For the purpose of accurately quantifying forest GSV in vast acreages of land, a remotely sensed mosaic is an effective and available tool, particularly if novel methodologies with better performance are proposed, to overcome time-consuming and laborious difficulties obtained by area-based data collection [3]. There are ever-growing numbers of remote sensing techniques, especially for airborne light detection and ranging (LiDAR) and unmanned aerial vehicle (UAV) platforms, which have been demonstrated to be of great interest for forest parameter predictions [4,5]. Nevertheless, expensive budgets for wide areas [3] and intricate processing [6] limit the practical applications of LiDAR and UAVs. Remote sensing based on satellite is a cardinal approach to monitor or evaluate forest characteristics across areas at relatively large geographic scales.

As a fine-resolution (up to 10 m) Earth observation satellite pair and with a high revisit of five days, Sentinel-2 (S2) is a publicly-accessible and free resource providing systematically global coverage of land surfaces [7]. Previous studies have accepted that S2 Multispectral Instrument (MSI) performed extremely well in forecasting wide varieties of forest parameters. The authors of [8] acquired S2 and Landsat 8 (L8) data to predict forest

GSV in the Mediterranean and concluded that S2 (R^2 = 0.63) marginally outstripped L8 (R^2 = 0.62) and that the vegetation index derived from the red-edge band B5 of S2 remarkably correlated with GSV. By utilizing S2 MSI mosaic to estimate GSV for Lazio and Tuscany in Italy, [9] also reported that S2 achieved less than 19% at root mean square difference (RMSD) of both study areas. Consequently, Sentinel-2 satellite images of this paper were obtained from Copernicus Open Access Hub (https://scihub.copernicus.eu/, accessed on 4 May 2018) to apply to the forest GSV prediction.

Both vegetation indices and texture measures derived from optical sensors have been demonstrated to play a momentous role when evaluating forest parameters [3,5,10]. Many vegetation indices have been considered a sort of indispensable predictor and employed to monitor vegetation properties across various kinds of global ecological research since the 1970s [11]. For example, the Normalized Difference Vegetation Index (NDVI) has been used for investigating temporal variations in the Amazon forest [12]. Moreover, the vegetation spectral indices derived from disparate sensor bands might show different associations with different forest stand variables, depending on the complexity of the forests [10]. Texture measures have no rigorous definition and usually took into account visually complicated patterns that constitute entities or sub-patterns [13]. The research referred to textural features that have demonstrated their capabilities for estimating mature or successional forest biomass [14] or GSV [15,16]. Researchers have proposed that image texture from NDVI could better capture variation in habitat [17] and was strongly associated with variation in bird species richness and micro-habitat diversity [18]. Nevertheless, little attention has been paid to the texture measures derived from a vegetation index for predicting GSV.

In addition, the importance of pixel values in predicting forest GSV has not been studied before. The authors of [19] reported that standard deviation characterizes broad-scale variability in habitat structure and was more strongly associated with species richness than mean values at the plot level. Since few studies have simultaneously investigated the summary statistics at plot level for forest GSV estimation, we also investigated different statistics at pixel level for our available survey plots. Generally speaking, (1) the existing research did not consider the competence of the vegetation indices-based texture measures, (2) and the performance of satellite imagery based on different pixel values, (3) and the combinations encompassing the above two points, for estimating GSV.

Consequently, the target of our research was to explore standard deviation or mean statistics at plot level and whether the texture measures from the vegetation index are conducive to GSV inversion. Specifically, the spectral predictors and textural measures encompassing mean values and standard deviations were examined. Moreover, we investigated ten feature sets consisting of different predictors and texture measures derived from spectral predictors (bands or vegetation indices). Masson pine (*Pinus massoniana*) and theropencedrymion were detected in our study to investigate the differences between different tree species.

2. Study Area and Materials

2.1. Study Site

In our research, the test zone (Figure A1, Appendix A) is Anji County (30°23′–30°53′N, 119°14′–119°53′E), which is situated in the northwest of Zhejiang Province, eastern China. Occupying an area of 188,571 ha, the general elevation is between 800 and 1500 m in Anji, which is topographically characterized by higher landforms in the southwest and lower in the northeast [20].

With 1423.4 mm and 16.1 °C average annual precipitation and temperature, respectively, Anji County has a relatively humid and warm climate and four remarkably variational seasons [21]. Approximately 70% of Anji is covered with subtropical forests. The staple vegetation genres in Anji County are dominated by evergreen broadleaved forest, theropencedrymion forest, and semitropical bamboo forest.

2.2. Field Sampleing

In this paper, the forest information of test plots was investigated by the Anji Forestry Bureau in 2018. In our study, the research plots were set by taking the forest resource survey and management into account. They were divided according to the terrain boundary (e.g., mountain ridges, valleys, roads, etc.) and the similar tree species, which were also summarized as dominant tree species. Dominant tree species appertain to the tree species with a proportion of GSV equal to or more than 65% of total GSV in a plot. The survey plots were built in the field by applying stratified random sampling, with the help of remotely sensed data whose spatial resolution is better than 2.5 m.

Those plots whose mean diameter at breast height was less than 5 cm were removed. Moreover, the entire area of our test sites is approximately 11,451,264 ha. In the meanwhile, two tree species—Masson pine (*Pinus massoniana*) and theropencedrymion were detected in our research to investigate whether the models would perform differently between the complicated forest stand with higher heterogeneity and the simple one. The summary information about our survey plots is displayed in Table 1.

Table 1. Summary census of forest variables for several dominant species.

Forest Variable	Masson Pine		Theropencedrymion		All Plots	
	Mean	Stdev	Mean	Stdev	Mean	Stdev
Number of stems (stems/ha)	847	316	1150	589	1275	948
Number of plots	1808		1214		14,271	
Age (year)	35.39	7.39	30.53	9.48	29.09	9.13
Canopy Cover (%)	72.01	12.25	74.02	11.31	73.29	10.76
GSV (m^3/ha)	102.28	45.93	74.55	37.34	75.11	52.08

2.3. Satellite Data

In this research, we employed two Sentinel-2 (S2) MSI images of the survey field from the European Space Agency (https://scihub.copernicus.eu/, accessed on 4 May 2018). The scenes of S2, which were two Level-1C orthorectified and top-of-atmosphere products, were implemented using an atmospheric correction in SEN2COR (version 2.9). We selected ten of thirteen bands in Sentinel-2 and ten generally utilized vegetation indices (four red-edge bands) that yield from S2 bands (Table 2). The vegetation indices have been utilized in previous research [5,8,15], which demonstrated their great performance for GSV prediction, especially for those based on red-edge bands. Moreover, standard deviation values (STD) and mean values (MV) were two image statistics for the GSV prediction.

Table 2. Bands and vegetation indices generated from S2 MSI for GSV modeling.

Bands/Vegetation Indices	Bands/Indices	Description
Bands	Band 2	Blue, 490 nm, 10 m
	Band 3	Green, 560 nm,10 m
	Band 4	Red, 665 nm, 10 m
	Band 5	Red edge, 705 nm, 20 m
	Band 6	Red edge, 749 nm, 20 m
	Band 7	Red edge, 783 nm, 20 m
	Band 8	Near infrared, 842 nm, 10 m
	Band 8A	Near infrared narrow, 865 nm, 20 m
	Band 11	Shortwave infrared 1, 1610 nm, 20 m
	Band 12	Shortwave infrared 2, 2190 nm, 20 m

Table 2. *Cont.*

Bands/Vegetation Indices	Bands/Indices	Description
Vegetation indices	NDVI	$\frac{B8-B4}{B8+B4}$ [22]
	SAVI	$\frac{B8-B4}{B8+B4+L} \times (L+1)$ $(where,\ L=0.5)$ [23]
	CIgreen	$\frac{B8}{B3}-1$ [24]
	SR	$\frac{B8}{B4}$ [25]
	DVI	B8 − B4 [25]
	NDII	$\frac{B8-B11}{B8+B11}$ [26]
Red-edge vegetation indices	MTCI	$\frac{B6-B5}{B5-B4}$ [27]
	MCARI	$((B5-B4)-0.2\times(B5-B3))\times\frac{B5}{B4}$ [28]
	NDVIre	$\frac{B8-B5}{B8+B5}$ [29]
	CIre	$\frac{B7}{B5}-1$ [24]

NDVI = Normalized Difference, Vegetation Index, SAVI = Soil Adjusted Vegetation Index, CIre= Red-edge Chlorophyll Index, SR = Simple Ratio, DVI = Difference vegetation Index, NDII = Normalized Difference Infrared Index, MTCI = MERIS terrestrial chlorophyll index, MCARI = Modified Chlorophyll Absorption Ratio Index, NDVIre = Red-edge NDVI, CIgreen = Green Chlorophyll Index.

First-order textural measures were figured out by primitive pixels. For all test plots, three first-order texture metrics (occurrence) of ten sensor bands as well as ten vegetation indices, including data range, mean, and variance, were calculated in our study. Furthermore, textural features were calculated from three processing window sizes: 5 × 5, 17 × 17, and 31 × 31. The texture measures were derived from ten spectral bands and ten vegetation indices, coupled with three kinds of texture metrics and three kinds of window sizes (e.g., $NDII_ME17_{SD}$ means the predictors were derived from NDII which combined the texture metrics 'mean' and the 17 × 17 window size, and the pixel values are STD). Additionally, the texture measures were computed in ENVI (version 5.3) using the formulas in Table 3.

Table 3. Texture metrics of bands/vegetation indices for GSV modeling.

Texture Metrics	Formula
Mean	$\frac{\sum_{k=1}^{N} x_k}{N}$ Where x_k represents the gray tone values of pixel k, N represents the number of gray tone values
Data range	$\max\{X\}-\min\{X\}$ Where X represents $x_1,\ x_2, \ldots,\ x_k$
Variance	$\frac{\sum_{k=1}^{N}(x_k-\bar{x})}{N-1}$

3. Methodology

3.1. Growing Stock Volume Modeling

Previous research has examined the sensitivity of the heterogeneity in vegetation and habitat taken by different pixel statistics using remotely sensed images, according to different variability of different statistical pixel results in the images [19]. In this research, standard deviation values (STD) and mean values (MV) of pixels acquired from the univariate predictors were applied to predict the GSV of three kinds of plots, so as to explore the difference between both pixel values to GSV inversion. Moreover, the textural metrics derived from bands and vegetation indices were also calculated to assess whether they yield different implications for different forest species. Eventually, ten feature sets were employed to detect the performance of different remotely sensed predictors (see Table 4).

In general, we first evaluated the relationships between in situ GSV and univariate predictors which encompassed original spectral bands, vegetation indices, and the texture measures. Two kinds of pixel values have been taken into account in all the predictors. Then, we built ten groups of combinations that comprised a variety of remote sensing data or patterns derived from raw data and utilized the feature importance of Random Forest to select four higher-ranking features to investigate the estimated competence with different kinds of predictors. The details are shown in Figure 1.

Table 4. Texture metrics of bands/vegetation indices for GSV modeling.

Experiment	Description
A: $S2_M$	All bands and vegetation indices based on MV
B: $S2_{SD}$	All bands and vegetation indices based on STD
C: $S2_M$ + $Bands_TM_M$	Synergizing all S2 predictors based on MV and texture measures derived from bands based on MV
D: $S2_M$ + $Bands_TM_{SD}$	Synergizing all S2 predictors based on MV and texture measures derived from bands based on STD
E: $S2_{SD}$ + $Bands_TM_M$	Synergizing all S2 predictors based on STD and texture measures derived from bands based on MV
F: $S2_{SD}$ + $Bands_TM_{SD}$	Synergizing all S2 predictors based on STD and texture measures derived from bands based on STD
G: $S2_M$ + VI_TM_M	Synergizing all S2 predictors based on MV and texture measures derived from vegetation indices based on MV
H: $S2_M$ + VI_TM_{SD}	Synergizing all S2 predictors based on MV and texture measures derived from vegetation indices based on STD
I: $S2_{SD}$ + VI_TM_M	Synergizing all S2 predictors based on STD and texture measures derived from vegetation indices based on MV
J: $S2_{SD}$ + VI_TM_{SD}	Synergizing all S2 predictors based on STD and texture measures derived from vegetation indices based on STD

Bands_TM and VI_TM, respectively, mean texture measures derived from spectral bands as well as vegetation indices. Subscript M represents the mean value of pixels, while SD represents the standard deviation value of pixels.

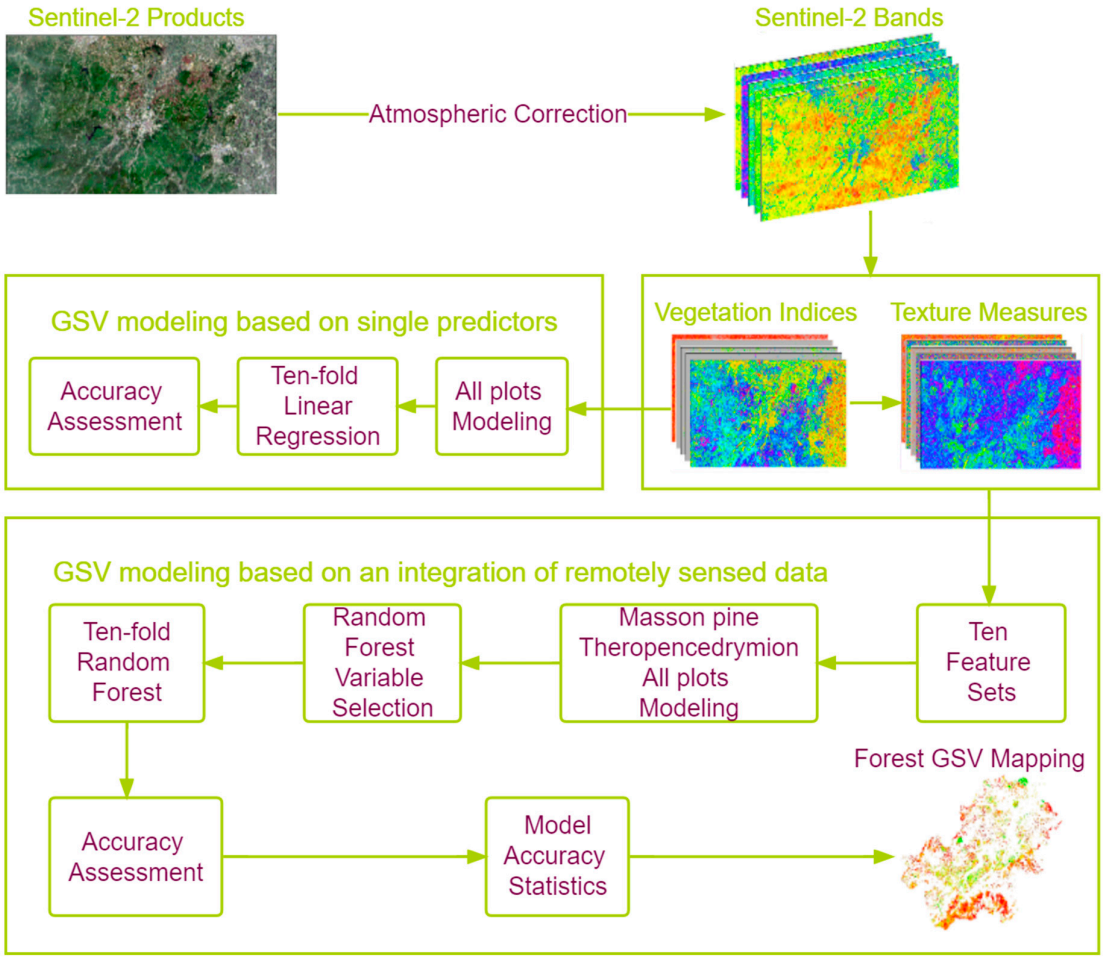

Figure 1. Flowchart of methodology for modeling growing stock volume.

3.2. Statistical Analyses for Modeling GSV

For the sake of evaluating the relationships between the univariate and GSV, Spearman's correlation as well as a parametric approach (linear regression, for univariate models) were exploited to establish GSV models. In addition, the Random Forest (RF) method was exploited in multivariate GSV models. Put forward by Breiman [30], Random Forest is an ensemble learning approach to advance the classification and regression trees (CART) containing an integration of numerous sets of remotely sensed predictors [31], according to a randomly screened subset of train samples and features [32]. Comparative research has reported that non-parametric approaches outperformed parametric approaches when predicting vegetation attributes [33,34]. Two hyperparameters related to Random Forests were modulated, comprising the number of trees (n_estimators) and the maximal depth of trees (max_depth). By aligning different hyperparameters, we select the best-performing hyperparameter sets to establish the responding GSV models. With mean square errors as predictive criteria, a grid search was applied in the "GridSearchCV" package to tune the optimal hyperparameters through ten-fold cross validation for RF models.

In this study, all GSV models were conducted in Anaconda using Python (version 3.8). Moreover, train sets and validated sets were extracted by a ten-fold cross-validation with five repetitions, which was employed to evaluate the performance of the models and ensure the robustness of the results for all GSV estimation models. The accuracy measures for GSV in the test sets encompass four criteria, which consist of correlation between the observed and predicted GSV values (r), coefficient of determination (R^2), the root mean square error (RMSE), and the relative RMSE (rRMSE). The criteria were calculated according to Equations (1)–(3):

$$R^2 = 1 - \frac{\sum_{i=1}^{N}(y_i - \hat{y}_i)^2}{\sum_{i=1}^{N}(y_i - \overline{y})^2} \quad (1)$$

$$RMSE = \sqrt{\frac{1}{N}\sum_{i=1}^{N}(y_i - \hat{y}_i)^2} \quad (2)$$

$$rRMSE = \frac{RMSE}{\overline{y}} \times 100\% \quad (3)$$

With y_i as the observed GSV values and $\overline{y}$ the mean of observed GSV values. $\hat{y}_i$ represents the estimated GSV values and N is the amount of test field plots.

4. Results

4.1. Relationships between In Situ GSV and Satellite Bands/Vegetation Indices

The outcomes estimated by the standard deviation values (STD) and mean values (MV) of bands/vegetation indices derived from Sentinel 2 and forest GSV were reported (Tables 5 and 6). Addionally, r in the table indicated the correlation coefficient obtained from the Spearman tests. It showed, remarkably, that an exceptional result was generated from CIre when predicting theropencedrymion, which might be attributed to variability or heterogeneity of complicated forest stands of theropencedrymion, and the results were exceptions when discussing the relationships between GSV and remotely sensed data.

Table 5. Estimated results for GSV of all plots using two measures of pixel value derived from satellite predictors.

Predicted Variables	Bands/ Indices	Standard Deviation				Mean			
		r	R^2	RMSE (m^3/ha)	rRMSE (%)	r	R^2	RMSE (m^3/ha)	rRMSE (%)
Bands	Band 2	−0.043 **	0.0003	52.04	69.29	−0.043 **	0.0007	52.03	69.28
	Band 3	0.032 **	−0.0006	52.07	69.32	−0.253 **	0.0407	50.98	67.88

Table 5. *Cont.*

Predicted Variables	Bands/ Indices	Standard Deviation				Mean			
		r	R^2	RMSE (m^3/ha)	rRMSE (%)	r	R^2	RMSE (m^3/ha)	rRMSE (%)
	Band 4	−0.057 **	0.0007	52.03	69.28	−0.055 **	0.0014	52.01	69.25
	Band 5	0.078 **	0.0015	52.01	69.25	−0.319 **	0.0678	50.26	66.91
	Band 6	−0.037 **	0.0003	52.04	69.29	−0.375 **	0.1070	49.19	65.46
	Band 7	−0.062 **	0.0021	51.99	69.23	−0.365 **	0.0995	49.39	65.76
	Band 8	−0.040 **	0.0003	52.04	69.29	−0.375 **	0.1080	49.16	65.45
	Band 8A	−0.049 **	0.0011	52.02	69.27	−0.369 **	0.1024	49.31	65.65
	Band 11	0.135 **	0.0062	51.89	69.09	−0.351 **	0.0985	49.42	65.80
	Band 12	0.010	−0.0005	52.06	69.32	−0.236 **	0.0374	51.07	67.99
Vegetation Indices	NDVI	−0.040 **	−0.0014	52.09	69.35	−0.176 **	0.0085	51.83	69.01
	SAVI	−0.040 **	−0.0014	52.09	69.35	−0.176 **	0.0085	51.83	69.01
	CIre	−0.084 **	−0.0006	52.07	69.32	−0.153 **	−0.0006	52.07	69.33
	SR	−0.187 **	0.0281	51.31	68.32	−0.203 **	0.0283	51.31	68.31
	DVI	−0.107 **	0.0005	52.04	69.29	−0.343 **	0.0876	49.72	66.19
	NDII	−0.028 **	−0.0007	52.07	69.33	−0.092 **	−0.0007	52.07	69.33
	MTCI	−0.016	−0.0010	52.08	69.34	−0.047 **	−0.0005	52.06	69.32
	MCARI	−0.047 **	−0.0002	52.06	69.31	−0.316 **	0.0761	50.03	66.61
	NDVIre	−0.020 *	−0.0005	52.06	69.32	−0.143 **	0.0027	51.98	69.21
	CIgreen	−0.125 **	−0.0005	52.06	69.32	−0.190 **	−0.0008	52.07	69.33

Parameter r represents the correlation coefficient between the predictors and GSV using Spearman tests. * Significance at the 5% level (two-tailed). ** Significance at the 1% level (two-tailed).

Table 6. Correlations and estimated results for GSV of two tree species using satellite predictors based on two pixels' statistics.

Predicted Variables	Bands/ Indices	Masson Pine				Theropencedrymion			
		Standard Deviation	$rRMSE_{SD}$ (%)	Mean	$rRMSE_M$ (%)	Standard Deviation	$rRMSE_{SD}$ (%)	Mean	$rRMSE_M$ (%)
Bands	Band 2	−0.166 **	44.52	0.064 **	44.90	−0.233 **	48.86	0.042	49.87
	Band 3	−0.135 **	44.53	−0.036	44.72	−0.181 **	49.14	−0.029	49.73
	Band 4	−0.205 **	44.24	−0.043	44.63	−0.269 **	48.67	−0.069 *	49.51
	Band 5	−0.167 **	44.39	−0.156 **	44.13	−0.204 **	49.13	−0.158 **	49.20
	Band 6	−0.094 **	44.70	−0.060 *	44.85	−0.070 *	50.00	−0.035	49.83
	Band 7	−0.085 **	44.74	−0.053 *	44.87	−0.080 **	50.00	−0.029	49.81
	Band 8	−0.079 **	44.76	−0.075 **	44.82	−0.057 *	50.00	−0.047	49.85
	Band 8A	−0.074 **	44.77	−0.059 *	44.86	−0.067 *	50.00	−0.040	49.84
	Band 11	−0.229 **	43.69	−0.231 **	43.61	−0.258 **	48.59	−0.263 **	48.97
	Band 12	−0.259 **	43.55	−0.205 **	43.71	−0.317 **	47.79	−0.255 **	48.84
Vegetation Indices	NDVI	−0.214 **	48.17	0.010	44.83	−0.263 **	50.90	0.046	49.62
	SAVI	−0.214 **	48.17	0.010	44.83	−0.263 **	50.90	0.046	49.62
	CIre	−0.108 **	44.89	0.062 **	44.94	−0.141 **	18.80	0.095 *	118.83
	SR	−0.218 **	43.96	−0.022	44.90	−0.290 **	48.70	0.005	49.84
	DVI	−0.142 **	46.22	−0.052 *	44.88	−0.142 **	49.63	−0.013	49.79
	NDII	−0.231 **	44.25	−0.043	44.66	−0.275 **	49.21	−0.006	49.82
	MTCI	−0.137 **	44.95	0.130 **	44.90	−0.193 **	49.81	0.161 **	49.83
	MCARI	−0.157 **	44.62	−0.111 **	44.65	−0.203 **	49.53	−0.052	49.87
	NDVIre	−0.198 **	44.86	0.074 **	44.70	−0.247 **	49.73	0.098 **	49.29
	CIgreen	−0.168 **	44.88	−0.046	44.99	−0.220 **	49.81	0.024	49.82

* Significance at the 5% level (two-tailed). ** Significance at the 1% level (two-tailed).

The MV of all plots obviously demonstrated a stronger correlation and better performance for GSV of all plots in comparison with the STD of pixels. The predicted rRMSEs ranged from 68.32% to 69.35% for STD of all plots, and from 65.45% to 69.33% for MV, which conspicuously exhibited the estimated potential of MV to be superior to STD. On the contrary, except for the outliers, the associations between satellite predictors within STD and

forest GSV were more striking than within MV, while the outperformed results using STD were close to MV for Masson pine and theropencedrymion. The best-performing predictors of STD were SR (rRMSE = 68.32%), and shortwave infrared 2 (SWIR2, rRMSE = 43.55%, 47.79%) for all plots, Masson pine and conifer–broadleaf forest, respectively, while the best of MV were near infrared (NIR, rRMSE = 68.31%), shortwave infrared 1 (SWIR1, rRMSE = 43.61%), and shortwave infrared 2 (SWIR2, rRMSE = 48.84%) for three kinds of plots. Obviously, NIR and SWIR offer the greatest interest in the forest stands, consistent with the previous reports [6,8]. Perhaps with structurally complicated plot attributes, it seemed that both theropencedrymion plots and all plots were tougher to predict than Masson pine.

4.2. Relationships between In Situ GSV and Texture Measures

With three different processing window sizes (5 × 5, 17 × 17, 31 × 31), three first-order texture metrics which encompassed two types of pixel statistics for all plots were calculated (Tables A1 and A2, Appendix B). In the meanwhile, the univariately evaluated relative RMSE employing texture metrics for Masson pine and theropencedrymion are exhibited in Figure 2.

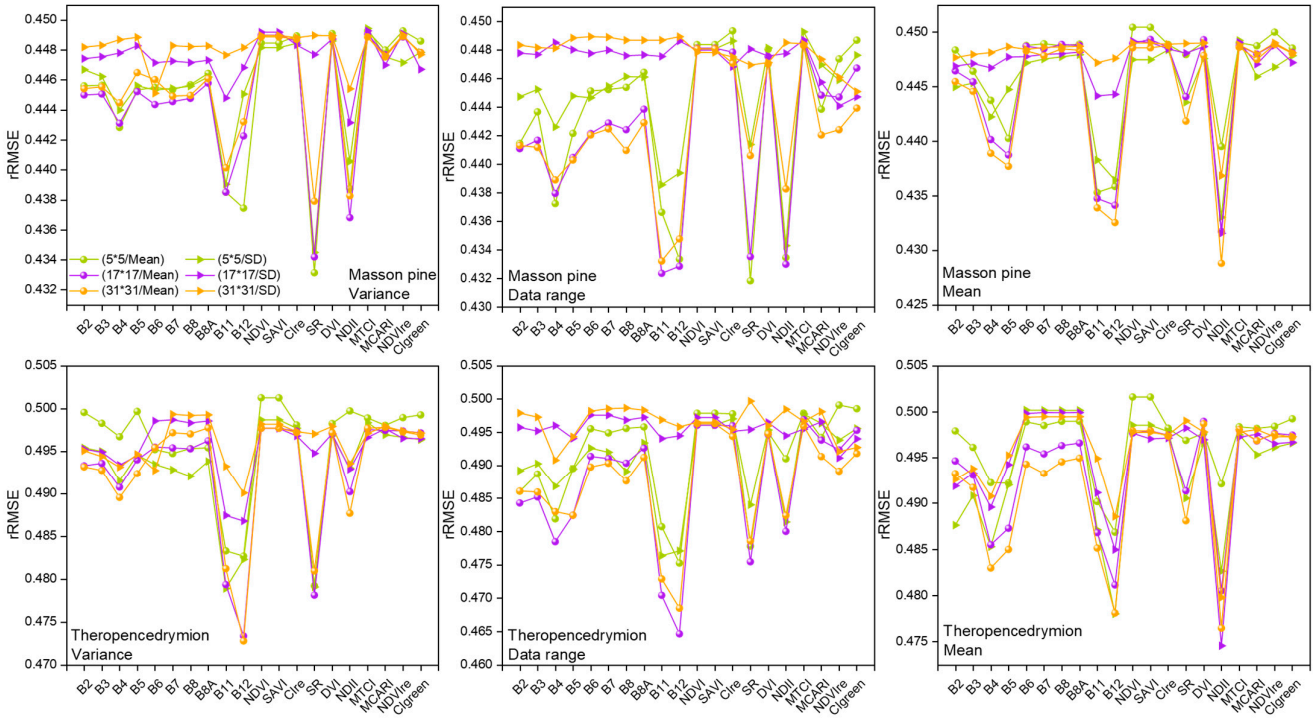

Figure 2. The estimated rRMSE of GSV using texture measures derived from remote sensing predictors for Masson pine and theropencedrymion. Mean in () of the first figure represents the mean statistics of pixel values, while SD represents the standard deviation. Variance, data range, and mean, which are displayed in the lower left or lower right corner, indicate three first-order texture measures.

It was noticeable that the range of predicted accuracies based on mean values (rRMSE = 42.88–45.05%, 46.47–50.16%, 65.99–69.33%) was a little wider than STD (rRMSE = 43.16–44.94%, 47.46–50.02%, 68.52–69.32%) for three kinds of plots. In the meantime, the best textural features of both statistics were NDII_ME31$_M$ (rRMSE = 42.88%), B12_ME17$_M$ (rRMSE = 46.47%), and B6_ME5$_M$ (rRMSE = 65.94%) for Masson pine, theropencedrymion, and all plots, respectively, while the worst were NDVI_ME5$_M$ and SAVI_ME5$_M$ (rRMSE = 45.05%), NDVI_ME5$_M$ and SAVI_ME5$_M$ (rRMSE = 50.16%), and MTCI_ME17$_M$ (rRMSE = 69.33%). The best and worst predictors were all from mean statistics.

For all plots, differentiated from those without remarkably pronounced window sizes for GSV estimation of Masson pine as well as theropencedrymion, more than half of the

best-performing processing window sizes of STD statistics were 31 × 31, while over half of satellite images with mean values were based on 5 × 5 window sizes. Above all, the well-performing texture measures were mainly based on the mean in 5 × 5 windows according to mean statistics (Table A2). Additionally, the better-fitting predictors were yielded from red-edge, NIR, and SWIR (rRMSE = 65.94–68.08%) based on mean pixel statistics. For Masson pine, several textural measures derived from SWIR, SR, and NDII in accordance with mean statistics exhibited greater performance. For theropencedrymion, in comparison to other texture features, more textures related to SWIR2 and NDII achieved higher accuracies. All in all, pattern textures within two pixels measures were close when predicting GSV. In addition, the upper limit of predictive potential for textures within mean values of pixels was slightly higher than STD.

4.3. GSV Modeling and Mapping Using Different Test Setups

Ten different feature sets were modeled to predict forest GSV for three kinds of survey plots (Table 7). Furthermore, utilizing the remotely sensed predictors by feature importance supported in RF, the models were ultimately established by the four most important variables (Table A3, Appendix C). Several groups of feature sets for all plots selecting remote sensing features are the same (groups A, C, D, G, H and group B, F); thus, only group A and group B were explored among these groups.

Table 7. Model results of the experimental groups based on Random Forest for three different survey plots.

Experiment	Survey Plots					
	Masson Pine		Theropencedrymion		All Plots	
	RMSE (m^3/ha)	rRMSE (%)	RMSE (m^3/ha)	rRMSE (%)	RMSE (m^3/ha)	rRMSE (%)
A	42.63	41.71	39.90	45.54	46.13	61.42
B	44.83	43.83	35.67	47.88	49.34	65.70
C	42.86	41.91	33.96	45.67	46.13	61.42
D	42.76	41.82	33.42	44.95	46.13	61.42
E	42.55	41.59	34.63	46.49	47.12	62.73
F	43.92	42.94	35.99	48.37	49.34	65.70
G	40.40	39.50	31.28	42.06	46.13	61.42
H	42.53	41.60	32.75	44.08	46.13	61.42
I	41.26	40.35	32.47	43.59	47.19	62.83
J	43.29	42.35	35.55	47.78	49.17	65.47

In a nutshell, the best-predicted forest was Masson pine and the worst one was all plots. The best predictors for estimating GSV of Masson pine, theropencedrymion, and all plots are selected by group G, group G, and group A, respectively, while the worst-performing groups are group B, group B, D, J, and group B, J, separately. The feature variables are all mean statistics of remotely sensed data and consist of textural measures based on VIs, VIs and bands for Masson pine, textural measures calculated from VIs for theropencedrymion, bands and VIs for all plots. On the contrary, the worst-performing predictors were mostly based on standard deviation statistics, except for group D of theropencedrymion. It should be noted that sensor spectral parameters took up the most crucial positions among all satellite predictors for all plots.

We also found that the selected feature variables in group I which had reached relatively higher accuracies were all VI-based textural measures for three kinds of plots. Another surprising consequence was that, although integrating with sundry texture measures, several groups of feature sets chose four identical spectral parameters (NIR, SWIR1, MTCI, MCARI), which manifested that texture measures had weaker competitiveness than spectral predictors to carry out GSV estimation for all plots.

In order to map forest growing stock volume for all available plots in our study, we selected the feature set achieving the best accuracy (rRMSE = 61.42%) from five repetition

models. The observed and estimated forest GSV patterns for all available plots in our study were displayed in Figure 3. Moreover, Figure 4 exhibits the scatterplots between observed and estimated GSV, showing the worst and the best models of three kinds of plots based on Table 7.

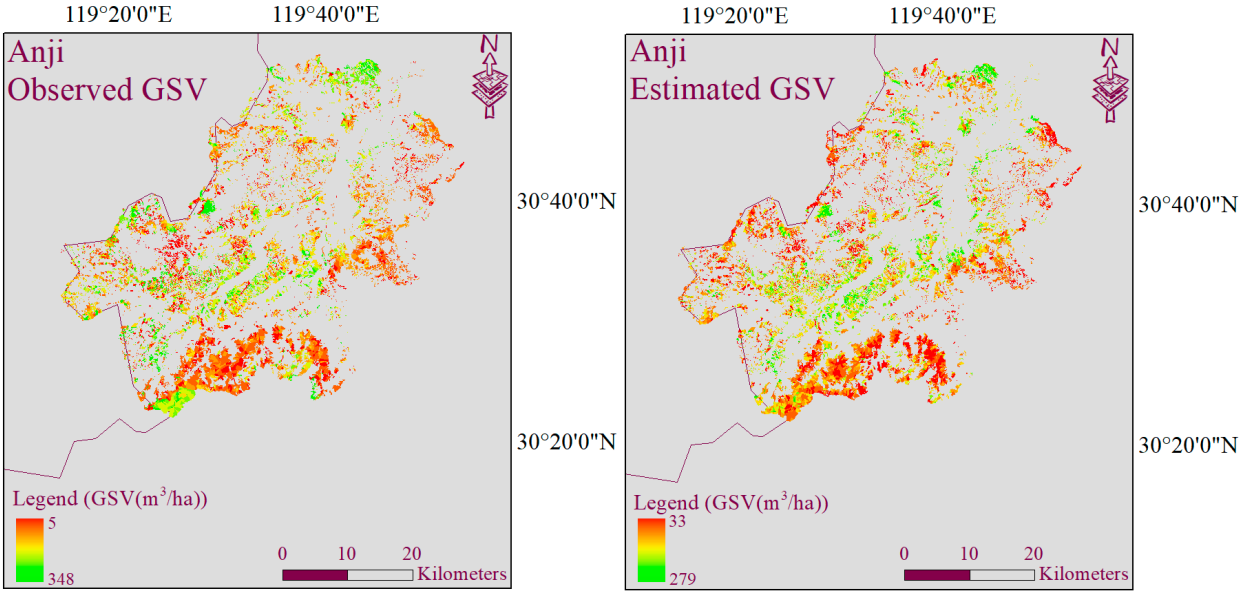

Figure 3. Observed and estimated GSV distribution maps of all plots.

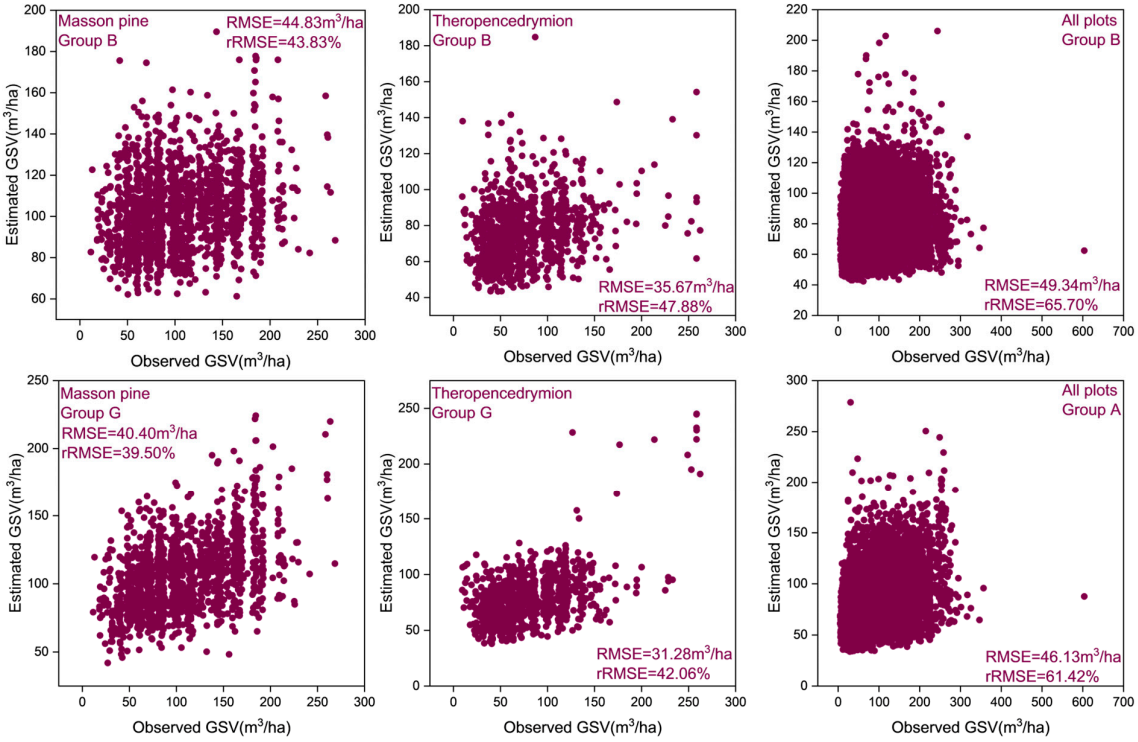

Figure 4. The scatterplots between observed and estimated GSV. The kinds of plots and the experimental groups are displayed in the top-left-hand corner or top-right-hand corner. The first row is the worst-performing models, while the second row is the best-performing models.

5. Discussion

In this research, we aimed to explore the discrepancy between two statistical methods and the significance in textural measures generated from bands and vegetation indices.

Moreover, we built ten groups of combinations that comprised a variety of remote sensing data or patterns derived from raw data and utilized the feature importance of Random Forest to select four higher-ranking features to investigate the estimated competence with different kinds of predictors.

5.1. Bands/VIs for Forest GSV Estimation

From the estimated results delineated in Tables 5 and 6, it could be deduced that the mean value slightly outstripped STD for all plots. Nevertheless, those predictors with measures of STD for estimating Masson pine and conifer–broadleaf showed that they were surrogates for those with mean values of pixels. Almost all predictors reported their inverse correlation with the GSV, no matter the kind of plots. There were lower associations between predictors and GSV when using mean measures of pixels. On the other hand, more predictors within mean values yielded better-predicted accuracies for all plots (e.g., B5, B8), while STD showed moderate performance among all remotely sensed variables.

We agreed with what previous work has put forward: that short-wave infrared band 1 (SWIR1) was a crucial indicator for GSV estimation [5,6]. The authors of [5] thought that the SWIR spectral band quantified tree canopy reflectance owing to the canopy cover of their considered survey plots being over 60%; the explanations also made sense in our research, according to our more than 70% canopy closure. In addition, the NIR band and red-edge bands also played an indispensable role in the GSV prediction of all plots, consistently with the foregoing study [8]. A surprising result should be noticed: that two dominant tree species only exhibited the critical role of SWIR, while other predictors have very little dissimilarity. This might be attributed to the greater contribution made to satellite remote sensing by the tree canopy of both dominant species compared with other forest parameters.

5.2. Texture Measures for GSV Estimation

In our study, image texture exploited its great competence in GSV estimation. There were no first-order textural metrics or moving window sizes that could summarize the estimation of GSV for different levels of plots. Moreover, the texture measures, no matter whether with STD or mean values, seemed not to deliver a pronounced conspicuous performance for GSV prediction.

For both Masson pine and conifer–broadleaf forests, an interesting result was that there were dozens of texture measures outperforming all the spectral parameters (e.g., $rRMSE_{Masson\ pine}$ (SR_VA5_{ME} (43.32%), $NDII_RA5_{SD}$ (43.43%), $B12_VA31_{ME}$ (43.26%)) < 43.55%, $rRMSE_{theropencedrymion}$ ($B12_VA31_{ME}$ (47.28%), $NDII_ME17_{SD}$ (47.46%), SR_RA17_{ME} (47.55%)) < 47.79%), especially the textures based on SWIR, NDII, and SR, albeit without an emphasis on any window sizes of image texture for two tree species. Similarly to the results reported by [15], who estimated the GSV of the Mediterranean, the performance offered by textural measures was superior to raw spectral bands/indices. The great performance stems from pattern textures that, based on vegetation indices, demonstrated that surrogate VI-based texture measures are equipped with better potential than spectral predictors to forecast forest GSV. In the investigation of [17], the authors pointed out that NDVI-based texture measures were adept at predicting variation in the habitats of large fields, and the conclusion was the resemblance to our survey objects. Moreover, NDII was based on NIR and SWIR1, while SR consists of the red band and NIR. Both of them have shown their strong performance for forest parameter estimation in previous work [6,8]. Consequently, it is plausibly indicated that the distribution characteristics of spectral intensities in a given neighborhood [19,35] computed from sensitive parameters in specific biophysical activities [36] could well explain those species of a forest stock volume with a high canopy, particularly for those satellite predictors that have been reckoned to have powerful potential for predicting vegetation structure. Last, but not least, in contrast with what [14] have reported, too large window sizes 31 × 31 clearly did not fit worse than other smaller windows; we ascribed this to the lesser vegetation variation as well as the

lesser texture variation than is shown in tropical vegetation in the plots of Masson pine and conifer–broadleaf.

For all plots, an interesting detection was that many predicted results seemed to have a regular change (increase or decrease), along with the enlargement or diminishment of window sizes, for standard deviation and mean statistics. From all predicted GSV consequences, however, it was shown that smaller windows have a stronger competence to create a better fit. This was analogous to what [37] investigated: the texture element of a small sliding window size from high-resolution imagery showing a better association with a horizontal vegetation structure. We also found that those textures achieving higher accuracies were based on red-edge, NIR, and SWIR, which have also been taken into account as immense spectral predictors for vegetation attributes prediction [8,38]. Thus, we deduce that it is valuable to allow for texture measures derived from those spectral parameters that have a great potential to predict forest characteristics.

Generally speaking, for single tree species, forest stocks were easier and cheaper to capture by satellite remote sensing, especially given the increasing numbers of open access satellites in recent years [39]. Furthermore, the best sliding window sizes for all available survey plots concentrated more regularly on the biggest or smallest sizes than on single tree species. The mean value at the plot level outperformed the standard deviation for GSV prediction. In addition, it was emphasized that the texture measures generated from SWIR or SWIR-based VI were to be adopted in the forest stock study.

5.3. Multivariate Models for GSV Estimation and Mapping

From the outcomes of ten variable sets for three levels of plots, group G displayed the strongest performance among all feature sets for Masson pine and conifer–broadleaf forests. Furthermore, the results also showed that the screened features in a couple of groups were coincidental for all plots, e.g., group A, C, D, G, H, group B, F, which manifested the robustness and stability of Random Forest for ranking feature importance. Different levels of the available sample plots also showed varied difficulty of predictions, according to the complexity and diversity generated from the vegetation.

For two forest species, it was obvious that the strongest-fitting group was based on textural measures and spectral predictors, which encompassed two textures derived from spectral bands and two spectral predictors for Masson pine, and all textural measures for conifer–broadleaf forests. The capacity of texture measures for GSV prediction was more powerful than that of spectral predictors. The top two best-fitting groups (groups G and I) almost constitute image textures. As a sort of feature variable that has been considered to be conducive to monitoring species richness [17,19,37], image texture measures exactly fulfilled a more significant role in mixed conifer and broadleaf vegetation with higher plot-level variability. For Masson pine, spectral elements still support help for reaching the best accuracies, albeit screened remotely sensed elements only encompassing red band and MTCI. Given the much more complicated structures and greater heterogeneity of conifer–broadleaf forest compared to Masson pine, the satellite mosaics unsurprisingly found the recording of forest stocks of the former more difficult. As with univariate models, the image textures based on NDII have become key variables again for both tree species.

For all available plots we detected, the best predictors were all on the basis of spectral parameters (A, C, D, G, H). Compared with univariate textural metrics, on the contrary, processing window sizes 5×5 reached the highest accuracies, which stems from mean pixel census. Thus, when considering which moving window size would be the best size, we found that it depends on tree species, pixel statistics, variable constraint conditions, and so on. On the other hand, pattern texture measures with smaller moving window sizes have been proved worth considering, which was consistent with previous studies [14,40]. Although selected from different data sets, predictors from several subsets (groups A, C, D, G, H) showed no differences and acquired the best precision. This illustrated that NIR, SWIR 1, MTCI, and MCARI could better summarize the characteristics of GSV of all plots.

Ultimately, one result (rRMSE = 61.42%) of five repetition models was adopted for mapping forest GSV.

All in all, texture measures offered to be very useful in predicting forest stocks. Another point that should be noted was that texture metrics derived from vegetation indices were a kind of promising remotely sensed feature for forest stock volume evaluation and was recommended to be taken into account in any other forest characteristics evaluation [3]. The statistical limit at the pixel level for forest stock prediction was low on the whole, and the mean values slightly outstripped the standard deviation. We also agreed with the perspective presented by [41], who employed MODIS satellite data to map the forest biomass across Russia, which was that the number of plots was not the limitation of better prediction ($Number_{theropencedrymion} < Number_{Masson\ pine} < Number_{all\ plots}$). The best accuracies were close to 60% for both of the dominant tree species, while it verged on 40% for all plots. The satellite-based predictive errors were poorer than Airborne scanning LiDAR, at about 30% RMSE [42] and were close to 59.3% acquired by Sentinel-2 [6]. We therefore supposed that it might be because sundry vegetation conspicuously yielded more remotely sensed noise than distinguished forest plots [43–45]. Using Random Forest as vegetation parameter, predictive tools have become popular [33,46], and the feature importance ranking supported by RF also helps researchers clearly to understand the significance of those higher-ranking predictors and to determine to reduce the redundancy of feature variables [47]. We did not exploit other machine learning models, so it is probably a promising approach to use other statistical algorithms in conjunction with any other relative variables, e.g., a digital elevation model (DEM), to implement forest GSV estimation.

5.4. Mean Value and Standard Deviation at Plot Level

In previous studies, the forest GSV models mostly employed the mean value of satellite imagery as the feature variable. We were also in line with the perspective in most of the forest GSV models in this paper. However, forest structure was complex and easily disturbed by understory resources [10] or other disturbance indicators [3] when using satellite imagery. The landscape heterogeneity of the forest thus contributed to the influence of spatial noise [19] and abnormal distribution of the recorded sensor patterns. The mean values at the plot level can also be ascribed to the biased forecast of forest stock volume [47].

The standard deviation is not skewed by considerable or quite small values and has been characterized by broad-scale variability in habitat structure [19]; thus, it might be a robust statistic when satellite image data showed abnormal distribution. Our research also found it available in the GSV models based on raw spectral data. Consequently, we suggest standard deviation be employed at the plot level for subsequent forest research using remotely sensed data.

6. Conclusions

Our work focused on investigating how different the predicted results would be between the plot-level mean value and standard deviation value for GSV inversion. Moreover, texture elements derived from spectral bands as well as vegetation indices were also explored. The survey plots were in Anji County, consisting of Masson pine, theropencedrymion, and all plots which included a variety of dominant tree species.

The SWIR-based vegetation index and the textures derived from SWIR or SWIR-based vegetation index were highlighted for their function for observing forest stock. The predicted GSV results showed that texture measures have a great potential as a surrogate predictor for capturing unitary tree species. We also found that VI-based texture metrics that were rarely adopted for forest parameter evaluations displayed a strong capacity for forest stock prediction. The well-fitting predictors for predicting forest stock volume were mostly based on texture metrics derived from the vegetation index. Consequently, we cast a promising light on mean statistics at the plot level as well as texture measures

based on vegetation indices when carrying out forest GSV predictions, even for any other vegetation variables. On the other side, we advise that standard deviation at the pixel level be applied to extensive studies on original satellite spectral parameters for examining vegetation. Eventually, we would encourage many other statistical algorithms as well as other correlative features (e.g., DEM) about vegetation parameters to be integrated with VI-based image textures for further research.

Author Contributions: Conceptualization, G.F.; methodology, G.F.; data curation, G.F.; writing—original draft preparation, G.F.; writing—review and editing, L.F.; Funding acquisition, L.F.; Investigation, X.H.; Supervision, Y.W. All authors have read and agreed to the published version of the manuscript.

Funding: This research was funded by Zhejiang Provincial Key Science and Technology Project, grant number 2018C02013.

Institutional Review Board Statement: Not applicable.

Informed Consent Statement: Not applicable.

Data Availability Statement: The data was supported by the Anji Forestry Bureau.

Conflicts of Interest: The authors declare no conflict of interest.

Appendix A

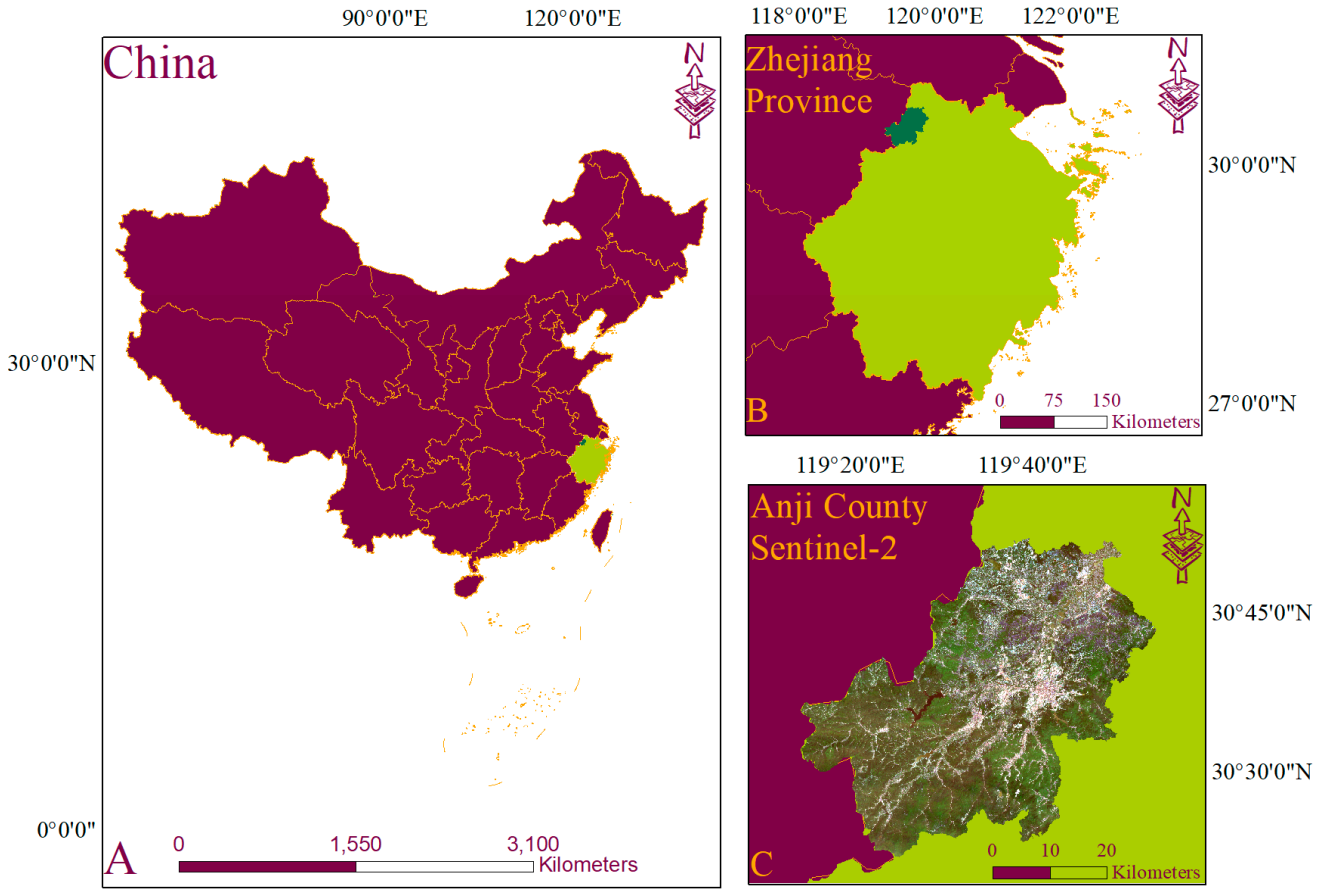

Figure A1. (**A**) represents the location of Zhejiang Province in China. (**B**) represents the geographical location of Anji County in Zhejiang Province. (**C**) represents the imagery of Sentinel-2 of Anji County, respectively.

Appendix B

Table A1. Results from univariate models of the standard deviation of first-order texture measure from band/vegetation index at different moving window sizes.

Bands/VIs	Variance			Data Range			Mean			RMSE (m^3/ha)	r	*p*
	5 × 5	17 × 17	31 × 31	5 × 5	17 × 17	31 × 31	5 × 5	17 × 17	31 × 31			
Band 2	69.33	69.32	69.30	69.33	69.28	69.27	69.32	69.30	**69.25**	52.01	0.078	<0.01
Band 3	69.32	69.29	69.26	69.32	69.26	69.26	69.30	69.21	**69.15**	51.93	0.110	<0.01
Band 4	69.33	69.29	69.24	69.33	**69.22**	69.23	69.31	69.30	69.23	51.99	0.096	<0.01
Band 5	69.29	69.21	69.17	69.24	69.20	69.20	69.21	69.13	**69.08**	51.88	0.116	<0.01
Band 6	69.23	69.32	**69.23**	69.29	69.30	69.24	69.30	69.32	69.33	52.00	−0.060	<0.01
Band 7	**69.20**	69.32	69.33	69.28	69.26	69.22	69.26	69.32	69.33	51.97	−0.073	<0.01
Band 8	**69.25**	69.33	69.33	69.32	69.30	69.27	69.27	69.32	69.33	52.01	−0.055	<0.01
Band 8A	69.24	69.33	69.33	69.30	69.27	**69.24**	69.29	69.33	69.33	52.00	0.095	<0.01
Band 11	69.28	69.24	69.22	69.27	69.23	69.23	**69.13**	69.19	69.21	51.92	0.124	<0.01
Band 12	69.33	69.26	69.21	69.33	**69.17**	69.23	69.33	69.30	69.25	51.95	0.090	<0.01
NDVI	69.33	69.30	69.27	69.33	69.28	**69.23**	69.33	69.31	69.30	52.00	0.093	<0.01
SAVI	69.33	69.30	69.27	69.33	69.28	**69.23**	69.33	69.31	69.30	52.00	0.093	<0.01
CIre	69.33	69.32	69.31	69.33	69.32	**69.28**	69.33	69.32	69.32	52.04	0.080	<0.01
SR	**68.52**	69.23	69.32	69.07	69.30	69.19	68.66	69.24	69.32	51.46	−0.153	<0.01
DVI	69.33	69.31	69.29	69.33	69.30	**69.27**	69.29	69.33	69.31	52.03	0.097	<0.01
NDII	69.14	69.32	69.29	69.31	69.14	**68.98**	69.28	69.30	69.32	51.81	0.113	<0.01
MTCI	69.33	69.33	69.32	69.33	69.33	**69.32**	69.33	69.33	69.32	52.06	0.084	<0,01
MCARI	69.32	69.32	69.32	69.33	69.28	**69.26**	69.30	69.33	69.33	52.02	0.069	<0.01
NDVIre	69.33	69.30	69.27	69.33	69.29	**69.24**	69.33	69.32	69.30	52.00	0.107	<0.01
CIgreen	69.33	69.31	69.29	69.32	69.29	**69.23**	69.32	69.32	69.30	52.00	0.101	<0.01

The results before RMSE are the rRMSE predicted by first-order textures based on different spectral parameters and three different window sizes. Moreover, based on the best predictors, the RMSE, the correlation coefficients (r) between the predictors and GSV using Spearman tests, and the *p*-value are displayed. The best estimated textural predictors of nine results in every line based on rRMSE are in bold.

Table A2. Results from univariate models of mean value of first-order texture measure from band/vegetation index at different moving window sizes.

Bands/VIs	Variance			Data Range			Mean			RMSE (m^3/ha)	r	*p*
	5 × 5	17 × 17	31 × 31	5 × 5	17 × 17	31 × 31	5 × 5	17 × 17	31 × 31			
Band 2	69.30	69.32	69.33	**69.25**	69.30	69.33	69.28	69.31	69.33	52.01	−0.051	<0.01
Band 3	69.33	69.32	69.31	69.33	69.33	69.33	**68.07**	68.73	68.98	51.13	−0.230	<0.01
Band 4	69.31	69.33	69.32	**69.21**	69.31	69.29	69.24	69.27	69.29	51.98	−0.064	<0.01
Band 5	69.30	69.26	69.23	69.30	69.31	69.29	**67.09**	67.97	68.41	50.38	−0.304	<0.01
Band 6	69.13	69.17	69.16	69.10	69.16	69.28	**65.94**	67.49	68.12	49.52	−0.355	<0.01
Band 7	69.02	69.10	69.20	68.95	69.10	69.27	**66.19**	67.65	68.23	49.71	−0.347	<0.01
Band 8	69.14	69.16	69.24	69.15	69.20	69.29	**65.99**	67.52	68.12	49.56	−0.354	<0.01
Band 8A	69.11	69.18	69.26	69.06	69.18	69.30	**66.06**	67.50	68.11	49.62	−0.353	<0.01
Band 11	69.30	69.31	69.30	69.26	69.31	69.31	**66.08**	67.21	67.72	49.63	−0.335	<0.01
Band 12	69.31	69.32	69.33	69.28	69.31	69.33	**68.08**	68.48	68.67	51.13	−0.221	<0.01
NDVI	69.33	69.32	69.31	69.33	69.33	69.31	**69.28**	69.33	69.33	52.04	−0.137	<0.01
SAVI	69.33	69.32	69.31	69.33	69.33	69.31	**69.28**	69.33	69.33	52.04	−0.137	<0.01
CIre	69.32	69.32	69.33	**69.32**	69.33	69.33	69.32	69.32	69.33	52.07	−0.102	<0.01
SR	68.27	68.55	68.84	**68.15**	68.77	69.10	68.58	69.05	69.16	51.18	−0.178	<0.01
DVI	69.33	69.33	69.32	69.28	69.33	69.32	**66.96**	68.95	69.19	50.29	−0.315	<0.01
NDII	69.30	69.29	69.29	69.24	69.31	69.32	69.27	69.16	**69.14**	51.93	−0.021	0.011
MTCI	69.33	69.33	69.33	69.33	69.33	69.33	69.33	**69.33**	69.33	52.07	0.026	0.002
MCARI	69.33	69.33	69.33	69.29	69.33	69.33	**67.49**	68.76	69.01	50.69	−0.282	<0.01
NDVIre	69.33	69.33	69.32	69.32	69.33	69.32	**69.30**	69.33	69.33	52.05	−0.111	<0.01
CIgreen	69.33	69.33	69.33	69.33	69.32	**69.31**	69.33	69.33	69.33	52.06	0.012	0.148

The results before RMSE are the rRMSE predicted by first-order textures based on different spectral parameters and three different window sizes. Moreover, based on the best predictors, the RMSE, the correlation coefficients (r) between the predictors and GSV using Spearman tests, and the *p*-value are displayed. The best estimated textural predictors of nine results in every line based on rRMSE are in bold.

Appendix C

Table A3. Feature variables screened by Random Forest for three tree species taking advantage of ten feature sets.

Experiment	Tree Species		
	Masson Pine	**Theropencedrymion**	**All Plots**
A	$S2_B11_M$ (12.24), $S2_B2_M$ (10.82), $MTCI_M$ (8.03), $S2_B3_M$ (6.13)	$S2_B12_M$ (11.06), $S2_B2_M$ (10.21), $MTCI_M$ (9.44), $S2_B11_M$ (8.24)	$S2_B8_M$ (14.02), $S2_B11_M$ (9.16), $MTCI_M$ (7.35), $MCARI_M$ (7.33)
B	$S2_B12_{SD}$ (8.89), SR_{SD} (8.16), $NDII_{SD}$ (7.47), $MCARI_{SD}$ (6.92)	$S2_B12_{SD}$ (14.84), $CIgreen_{SD}$ (7.55), SR_{SD} (7.04), $MTCI_{SD}$ (6.72)	SR_{SD} (10.4), $S2_B11_{SD}$ (8.17), $MCARI_{SD}$ (7.43), $CIgreen_{SD}$ (6.1)
C	$B11_RA17_M$ (4.46), $MTCI_M$ (4.74), $MCARI_M$ (3.65), $B12_VA31_M$ (3.07)	$B12_VA31_M$ (7.62), $MTCI_M$ (6.91), $B12_RA31_M$ (3.22), $B12_VA17_M$ (3.1)	$S2_B8_M$ (12.13), $MCARI_M$ (3.58), $S2_B11_M$ (3.37), $MTCI_M$ (3.37)
D	$S2_B11_M$ (5.04), $S2_B2_M$ (3.76), $MTCI_M$ (3.69), $MCARI_M$ (2.94)	$MTCI_M$ (6.05), $B11_VA5_{SD}$ (4.98), $S2_B11_M$ (3.38), $S2_B2_M$ (3.05)	$S2_B8_M$ (3.65), $S2_B11_M$ (5.26), $MTCI_M$ (3.18), $MCARI_M$ (3.65)
E	$B11_RA17_M$ (4.46), $B2_ME5_M$ (3.06), $B12_VA31_M$ (2.8), $B11_ME31_M$ (2.29)	$B12_VA31_M$ (7.54), $B12_VA17_M$ (3.61), $B12_RA31_M$ (3.1), $B11_VA31_M$ (2.62)	$B8_ME5_M$ (9.53), $B11_ME5_M$ (5.58), $B5_ME31_M$ (2.33), $B6_ME5_M$ (1.97)
F	$B11_VA5_{SD}$ (3.41), SR_{SD} (3.2), $B4_ME5_{SD}$ (2.81), $MCARI_{SD}$ (2.34)	$B11_VA5_{SD}$ (4.6), $B11_RA5_{SD}$ (3.02), $B12_VA5_{SD}$ (2.83), $S2_B12_{SD}$ (2.74)	SR_{SD} (6.32), $S2_B11_{SD}$ (3.57), $MCARI_{SD}$ (3.12), $CIgreen_{SD}$ (2.29)
G	$NDII_ME31_M$ (12.22), $MCARI_ME31_M$ (3.2), $S2_B4_M$ (3.16), $MTCI_M$ (2.69)	$MTCI_ME31_M$ (4.42), $NDII_ME31_M$ (3.51), SR_RA31_M (3.42), $NDII_VA31_M$ (3.04)	$S2_B8_M$ (12.14), $S2_B11_M$ (4.48), $MTCI_M$ (3.47), $MCARI_M$ (2.49)
H	$NDII_ME17_{SD}$ (6.58), $NDII_ME5_{SD}$ (4.16), $MCARI_M$ (3.38), $MTCI_M$ (2.8)	$NDII_ME17_{SD}$ (6.47), $NDII_ME31_{SD}$ (6.4), $MTCI_M$ (5.87), $S2_B2_M$ (3.32)	$S2_B8_M$ (12.01), $S2_B11_M$ (4.68), $MCARI_M$ (3.68), $MTCI_M$ (3.01)
I	$NDII_ME31_M$ (11.94), $MTCI_ME31_M$ (3.83), SR_RA31_M (2.93), $MTCI_ME5_M$ (2.48)	$MTCI_ME31_M$ (4.6), SR_RA31_M (4.45), $NDVI_VA31_M$ (3.23), $NDVIre_VA31_M$ (3.3)	DVI_ME5_M (10.16), $MCARI_ME5_M$ (4), $MTCI_ME5_M$ (2.12), SR_VA5_M (2.11)
J	$NDII_ME17_{SD}$ (6.74), $NDII_ME5_{SD}$ (3.68), $S2_B4_{SD}$ (2.5), $NDII_ME31_{SD}$ (2.28)	$NDII_ME31_{SD}$ (8.01), $NDII_ME17_{SD}$ (4.5), $NDII_ME5_{SD}$ (2.17), $S2_B8_{SD}$ (1.9)	SR_{SD} (5.34), $S2_B11_{SD}$ (4.06), $MCARI_{SD}$ (2.38), $MCARI_VA5_{SD}$ (1.91)

VA, ME, and RA indicate variance, mean, and data range of first-order textural measures, respectively. 5, 17, and 31 indicate three different windows (5×5, 17×17, 31×31). SD and M indicate standard deviation and mean statistics of remotely sensed imagery pixels. The numbers in () indicate the proportion of variable importance of all remotely sensed predictors.

References

1. Santoro, M.; Beer, C.; Cartus, O.; Schmullius, C.; Shvidenko, A.; McCallum, I.; Wegmüller, U.; Wiesmann, A. Retrieval of growing stock volume in boreal forest using hyper-temporal series of Envisat ASAR ScanSAR backscatter measurements. *Remote Sens. Environ.* **2011**, *115*, 490–507. [CrossRef]
2. Seidl, R.; Schelhaas, M.-J.; Rammer, W.; Verkerk, P.J. Increasing forest disturbances in Europe and their impact on carbon storage. *Nat. Clim. Chang.* **2014**, *4*, 806–810. [CrossRef] [PubMed]
3. Ozdemir, I.; Karnieli, A. Predicting forest structural parameters using the image texture derived from WorldView-2 multispectral imagery in a dryland forest, Israel. *Int. J. Appl. Earth Obs. Geoinf.* **2011**, *13*, 701–710. [CrossRef]

4. Puliti, S.; Saarela, S.; Gobakken, T.; Ståhl, G.; Næsset, E. Combining UAV and Sentinel-2 auxiliary data for forest growing stock volume estimation through hierarchical model-based inference. *Remote Sens. Environ.* **2018**, *204*, 485–497. [CrossRef]
5. Sánchez-Ruiz, S.; Moreno-Martínez, Á.; Izquierdo-Verdiguier, E.; Chiesi, M.; Maselli, F.; Gilabert, M.A. Growing stock volume from multi-temporal landsat imagery through google earth engine. *Int. J. Appl. Earth Obs. Geoinf.* **2019**, *83*, 101913. [CrossRef]
6. Astola, H.; Häme, T.; Sirro, L.; Molinier, M.; Kilpi, J. Comparison of Sentinel-2 and Landsat 8 imagery for forest variable prediction in boreal region. *Remote Sens. Environ.* **2019**, *223*, 257–273. [CrossRef]
7. Drusch, M.; Del Bello, U.; Carlier, S.; Colin, O.; Fernandez, V.; Gascon, F.; Hoersch, B.; Isola, C.; Laberinti, P.; Martimort, P.; et al. Sentinel-2: ESA's Optical High-Resolution Mission for GMES Operational Services. *Remote Sens. Environ.* **2012**, *120*, 25–36. [CrossRef]
8. Chrysafis, I.; Mallinis, G.; Siachalou, S.; Patias, P. Assessing the relationships between growing stock volume and Sentinel-2 imagery in a Mediterranean forest ecosystem. *Remote Sens. Lett.* **2017**, *8*, 508–517. [CrossRef]
9. Mura, M.; Bottalico, F.; Giannetti, F.; Bertani, R.; Giannini, R.; Mancini, M.; Orlandini, S.; Travaglini, D.; Chirici, G. Exploiting the capabilities of the Sentinel-2 multi spectral instrument for predicting growing stock volume in forest ecosystems. *Int. J. Appl. Earth Obs. Geoinf.* **2018**, *66*, 126–134. [CrossRef]
10. Lu, D.; Chen, Q.; Wang, G.; Liu, L.; Li, G.; Moran, E. A survey of remote sensing-based aboveground biomass estimation methods in forest ecosystems. *Int. J. Digit. Earth* **2016**, *9*, 63–105. [CrossRef]
11. Zeng, Y.; Hao, D.; Huete, A.; Dechant, B.; Berry, J.; Chen, J.M.; Joiner, J.; Frankenberg, C.; Ben Bond-Lamberty, B.; Ryu, Y.; et al. Optical vegetation indices for monitoring terrestrial ecosystems globally. *Nat. Rev. Earth Environ.* **2022**, *3*, 477–493. [CrossRef]
12. Kobayashi, H.; Dye, D.G. Atmospheric conditions for monitoring the long-term vegetation dynamics in the Amazon using normalized difference vegetation index. *Remote Sens. Environ.* **2005**, *97*, 519–525. [CrossRef]
13. Chen, S.; Useya, J.; Mugiyo, H. Decision-level fusion of Sentinel-1 SAR and Landsat 8 OLI texture features for crop discrimination and classification: Case of Masvingo, Zimbabwe. *Heliyon* **2020**, *6*, e05358. [CrossRef] [PubMed]
14. Lu, D.; Batistella, M. Exploring TM Image Texture and its Relationships with Biomass Estimation in Rondônia, Brazilian Amazon. *Acta Amaz.* **2005**, *35*, 249–257. [CrossRef]
15. Chrysafis, I.; Mallinis, G.; Tsakiri, M.; Patias, P. Evaluation of single-date and multi-seasonal spatial and spectral information of Sentinel-2 imagery to assess growing stock volume of a Mediterranean forest. *Int. J. Appl. Earth Obs. Geoinf.* **2019**, *77*, 1–14. [CrossRef]
16. Li, X.; Liu, Z.; Lin, H.; Wang, G.; Sun, H.; Long, J.; Zhang, M. Estimating the Growing Stem Volume of Chinese Pine and Larch Plantations based on Fused Optical Data Using an Improved Variable Screening Method and Stacking Algorithm. *Remote Sens.* **2020**, *12*, 871. [CrossRef]
17. Wood, E.M.; Pidgeon, A.M.; Radeloff, V.C.; Keuler, N.S. Image Texture Predicts Avian Density and Species Richness. *PLoS ONE* **2013**, *8*, e63211. [CrossRef]
18. Ozdemir, I.; Mert, A.; Ozkan, U.Y.; Aksan, S.; Unal, Y. Predicting bird species richness and micro-habitat diversity using satellite data. *For. Ecol. Manag.* **2018**, *424*, 483–493. [CrossRef]
19. St-Louis, V.; Pidgeon, A.M.; Radeloff, V.C.; Hawbaker, T.J.; Clayton, M.K. High-resolution image texture as a predictor of bird species richness. *Remote Sens. Environ.* **2006**, *105*, 299–312. [CrossRef]
20. Nie, W.; Shi, Y.; Siaw, M.J.; Yang, F.; Wu, R.; Wu, X.; Zheng, X.; Bao, Z. Constructing and optimizing ecological network at county and town Scale: The case of Anji County, China. *Ecol. Indic.* **2021**, *132*, 108294. [CrossRef]
21. Zhang, J.; Ge, Y.; Chang, J.; Jiang, B.; Jiang, H.; Peng, C.; Zhu, J.; Yuan, W.; Qi, L.; Yu, S. Carbon storage by ecological service forests in Zhejiang Province, subtropical China. *For. Ecol. Manag.* **2007**, *245*, 64–75. [CrossRef]
22. JRouse, W.; Haas, R.H.; Schell, J.A.; Deering, W.D. Monitoring vegetation systems in the Great Plains with ERTS. *Third ERTS Symp.* **1973**, *351*, 309–317.
23. Huete, A. A soil-adjusted vegetation index (SAVI). *Remote Sens. Environ.* **1988**, *25*, 295–309. [CrossRef]
24. Gitelson, A.A.; Gritz, Y.; Merzlyak, M.N. Relationships between leaf chlorophyll content and spectral reflectance and algorithms for non-destructive chlorophyll assessment in higher plant leaves. *J. Plant Physiol.* **2003**, *160*, 271–282. [CrossRef]
25. Jordan, C.F. Derivation of Leaf-Area Index from Quality of Light on the Forest Floor. *Ecology* **1969**, *50*, 663–666. [CrossRef]
26. Hardisky, M.A.; Daiber, F.C.; Roman, C.T.; Klemas, V. Remote sensing of biomass and annual net aerial primary productivity of a salt marsh. *Remote Sens. Environ.* **1984**, *16*, 91–106. [CrossRef]
27. Dash, J.; Curran, P.J. The MERIS terrestrial chlorophyll index. *Int. J. Remote Sens.* **2004**, *25*, 5403–5413. [CrossRef]
28. Daughtry, C. Estimating Corn Leaf Chlorophyll Concentration from Leaf and Canopy Reflectance. *Remote Sens. Environ.* **2000**, *74*, 229–239. [CrossRef]
29. Gitelson, A.; Merzlyak, M.N. Spectral Reflectance Changes Associated with Autumn Senescence of *Aesculus hippocastanum* L. and *Acer platanoides* L. Leaves. Spectral Features and Relation to Chlorophyll Estimation. *J. Plant Physiol.* **1994**, *143*, 286–292. [CrossRef]
30. Breiman, L.E.O. Random Forests. *Mach. Learn.* **2001**, *45*, 5–32. [CrossRef]
31. Mutanga, O.; Adam, E.; Cho, M.A. High density biomass estimation for wetland vegetation using WorldView-2 imagery and random forest regression algorithm. *Int. J. Appl. Earth Obs. Geoinf.* **2012**, *18*, 399–406. [CrossRef]
32. Belgiu, M.; Dra, L. Random forest in remote sensing: A review of applications and future directions. *ISPRS J. Photogramm. Remote Sens.* **2016**, *114*, 24–31. [CrossRef]

33. Wang, J.; Xiao, X.; Bajgain, R.; Starks, P.; Steiner, J.; Doughty, R.B.; Chang, Q. Estimating leaf area index and aboveground biomass of grazing pastures using Sentinel-1, Sentinel-2 and Landsat images. *ISPRS J. Photogramm. Remote Sens.* **2019**, *154*, 189–201. [CrossRef]
34. Ndikumana, E.; Minh, D.H.T.; Nguyen, H.T.D.; Baghdadi, N.; Courault, D.; Hossard, L.; El Moussawi, I. Estimation of rice height and biomass using multitemporal SAR Sentinel-1 for Camargue, Southern France. *Remote Sens.* **2018**, *10*, 1394. [CrossRef]
35. Szantoi, Z.; Escobedo, F.; Abd-Elrahman, A.; Smith, S.; Pearlstine, L. Analyzing fine-scale wetland composition using high resolution imagery and texture features. *Int. J. Appl. Earth Obs. Geoinf.* **2013**, *23*, 204–212. [CrossRef]
36. Camps-Valls, G.; Campos-Taberner, M.; Moreno-Martínez, A.; Walther, S.; Duveiller, G.; Cescatti, A.; Mahecha, M.D.; Muñoz-Marí, J.; García-Haro, F.J.; Guanter, L.; et al. A unified vegetation index for quantifying the terrestrial biosphere. *Sci. Adv.* **2021**, *7*, eabc7447. [CrossRef]
37. Wood, E.M.; Pidgeon, A.M.; Radeloff, V.C.; Keuler, N.S. Image texture as a remotely sensed measure of vegetation structure. *Remote Sens. Environ.* **2012**, *121*, 516–526. [CrossRef]
38. Korhonen, L.; Hadi; Packalen, P.; Rautiainen, M. Comparison of Sentinel-2 and Landsat 8 in the estimation of boreal forest canopy cover and leaf area index. *Remote Sens. Environ.* **2017**, *195*, 259–274. [CrossRef]
39. Forkuor, G.; Zoungrana, J.-B.B.; Dimobe, K.; Ouattara, B.; Vadrevu, K.P.; Tondoh, J.E. Above-ground biomass mapping in West African dryland forest using Sentinel-1 and 2 datasets—A case study. *Remote Sens. Environ.* **2020**, *236*, 111496. [CrossRef]
40. Li, X.; Lin, H.; Long, J.; Xu, X. Mapping the Growing Stem Volume of the Coniferous Plantations in North China Using Multispectral Data from Integrated GF-2 and Sentinel-2 Images and an Optimized Feature Variable Selection Method. *Remote Sens.* **2021**, *13*, 2740. [CrossRef]
41. Houghton, R.A.; Butman, D.; Bunn, A.G.; Krankina, O.N.; Schlesinger, P.; Stone, T.A. Mapping Russian forest biomass with data from satellites and forest inventories. *Environ. Res. Lett.* **2007**, *2*, 045032. [CrossRef]
42. Kankare, V.; Vastaranta, M.; Holopainen, M.; Räty, M.; Yu, X.; Hyyppä, J.; Hyyppä, H.; Alho, P.; Viitala, R. Retrieval of Forest Aboveground Biomass and Stem Volume with Airborne Scanning LiDAR. *Remote Sens.* **2013**, *5*, 2257–2274. [CrossRef]
43. Zhou, R.; Wu, D.; Fang, L.; Xu, A.; Lou, X. A Levenberg–Marquardt Backpropagation Neural Network for Predicting Forest Growing Stock Based on the Least-Squares Equation Fitting Parameters. *Forests* **2018**, *9*, 757. [CrossRef]
44. Lu, D.; Mausel, P.; Brondı, E.; Moran, E. Relationships between forest stand parameters and Landsat TM spectral responses in the Brazilian Amazon Basin. *For. Ecol. Manag.* **2004**, *198*, 149–167. [CrossRef]
45. Zhao, Q.; Yu, S.; Zhao, F.; Tian, L.; Zhao, Z. Comparison of machine learning algorithms for forest parameter estimations and application for forest quality assessments. *For. Ecol. Manag.* **2019**, *434*, 224–234. [CrossRef]
46. Yu, X.; Ge, H.; Lu, D.; Zhang, M.; Lai, Z.; Yao, R. Comparative study on variable selection approaches in establishment of remote sensing model for forest biomass estimation. *Remote Sens.* **2019**, *11*, 1437. [CrossRef]
47. Macedo, F.L.; Sousa, A.M.O.; Gonçalves, A.C.; da Silva, J.R.M.; Mesquita, P.A.; Rodrigues, R.A.F. Above-ground biomass estimation for *Quercus rotundifolia* using vegetation indices derived from high spatial resolution satellite images. *Eur. J. Remote Sens.* **2018**, *51*, 932–944. [CrossRef]

Disclaimer/Publisher's Note: The statements, opinions and data contained in all publications are solely those of the individual author(s) and contributor(s) and not of MDPI and/or the editor(s). MDPI and/or the editor(s) disclaim responsibility for any injury to people or property resulting from any ideas, methods, instructions or products referred to in the content.